ELSEVIER

Journal of Organometallic Chemistry 646 (2002) 204–211

Journal of Organometallic Chemistry

www.elsevier.com/locate/jorganchem

Syntheses, structure, and Berry pseudorotation of ruthenium-, iron-, and cobalt-phosphorane complexes

Hiroshi Nakazawa *, Kazumori Kawamura, Tsuyoshi Ogawa, Katsuhiko Miyoshi *

Department of Chemistry, Graduate School of Science, Hiroshima University, Higashi-Hiroshima 739-8526, Japan

Received 20 July 2001; accepted 18 September 2001

Abstract

Transition metal complexes bearing a phosphorane fragment with two 3-methylcatecholate substituents, $Cp'(CO)_2M\{\overline{P(OC_7H_6O)_2}\}$ ($Cp' = \eta^5\text{-}C_5H_5$, $\eta^5\text{-}C_5Me_5$; $M = Ru$, Fe) and $L(CO)_3Co\{\overline{P(OC_7H_6O)_2}\}$ ($L = PPh_3$, PPh_2Me), were prepared. The X-ray structure of $(\eta^5\text{-}C_5Me_5)(CO)_2Ru\{\overline{P(OC_7H_6O)_2}\}$ was determined. From the variable-temperature ^{31}P-NMR studies, the activation parameters for Berry pseudorotation around the pentacoordinate phosphorus were determined and discussed.

Keywords: Metallaphosphorane; Hypervalent bonds; Berry pseudorotation; Activation parameters

1. Introduction

Pentacoodinate phosphorus compounds, phosphoranes, have attracted considerable attention because they have 3-center-4-electron bonds (hypervalent bonds) in the apical positions and are an interesting family of chemical species violating the octet rule [1]. One behavior of phosphoranes is apical–equatorial rearrangement, so called Berry pseudorotation [2]. Although barriers to Berry pseudorotation of several organophosphoranes have been evaluated [3], those of phosphorane having a transition metal fragment as a substituent, metallaphosphorane, have not been reported. In 1999, we found that a metallaphosphorane with two 3-methylcatecholate substituents on a phosphorane phosphorus is suitable to estimate a barrier to Berry pseudorotation from the variable-temperature ^{31}P-NMR studies, and reported the first activation parameters of Berry pseudorotation for a ruthenium phosphorane [4]. In this paper, we report the synthesis, structure, and activation parameters of Berry pseudorotation for iron, ruthenium, and cobalt phosphoranes with 3-methylcatecholate substituents.

2. Results and discussion

2.1. Berry pseudorotation process of metallaphosphorane

A metallaphosphorane having two 3-methylcatecholate substituents in addition to a transition metal fragment on a phosphorane phosphorus is suitable for investigation on a pseudorotation process. Scheme 1 shows a graph for possible isomers of the metallaphosphorane and the relationship among them through Berry pseudorotation according to the convention [2a]. The phosphorus is surrounded by a transition metal and four oxygens classified into two kinds of oxygens (O1 and O2, which are close to and far from the methyl substituent, respectively). A symbol in an oval is to denote a particular trigonal–bipyramidal (tbp) configuration by the apical atoms. An *underlined* symbol shows the optical isomer of the parent compound. An atom drawn between symbols next to each other shows a pivot atom about which pseudorotation converts one isomer into another. There are ten possible configurations, which can be linked by 11 Berry pseudorotations.

* Corresponding authors. Tel.: +81-824-247420; fax: +81-824-240729.

0022-328X/02/$ - see front matter
PII: S0022-328X(01)01263-3

2.2. Preparation of metallaphosphoranes

We newly prepared five metallaphosphoranes, all of which have two 3-methylcatecholate substituents on the phosphorus. These complexes are shown in Eqs. (1) and (2), together with **1a** reported previously [4].

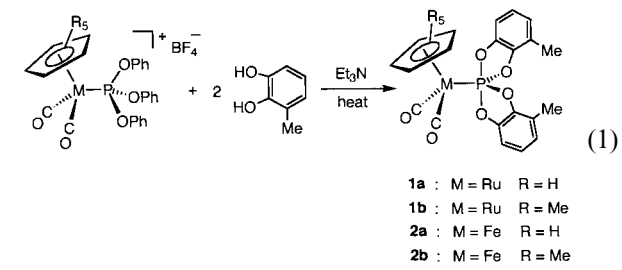

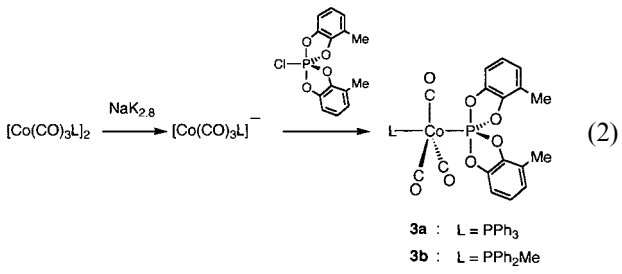

Ruthenium and iron phosphorane complexes (**1b**, **2a**, and **2b**) were prepared from $[Cp'(CO)_2M\{P(OPh)_3\}]^+$ ($Cp' = \eta^5$-C_5H_5 or η^5-C_5Me_5) and 3-methylcatechol in the presence of a base (Eq. (1)). In this reaction, nucleophilic attack of catecholate at the coordinating phosphite phosphorus takes place to give $Cp'(CO)_2M\{P(OC_7H_6O)_2\}$ [5] (although the complex should be described as $Cp'(CO)_2M\{\overline{P(OC_7H_6O)_2}\}$, the tie bar is omitted hereafter for simplicity). The product was isolated as a yellow powder in a moderate yield. The elemental analysis data showed that the isolated complexes were chemically pure metallaphosphoranes, but the spectroscopic data suggested a mixture of some isomers. In each case, the ^{31}P-NMR spectrum at room temperature shows two signals with an approximately equal intensity in the range of metallaphosphoranes. Due to equatophilicity of a transition-metal fragment, four isomers bearing a transition-metal fragment in an apical position (**MO1**, **MO2**, ***MO1***, and ***MO2***) can be ruled out as possible isomers of the isolated metallaphosphoranes. **O1O1** versus ***O2O2***, **O1O2** versus ***O1O2***, and **O2O2** versus ***O1O1*** are interconvertible by one transformation pathway with the transition-metal fragment in an equatorial position as a pivotal group. Therefore, two isomers in each pair are not distinguished in NMR spectra at room temperature. The interconversion between **O1O2** and ***O1O2*** corresponds to enantiomerization. **O1O1**/***O2O2*** is enantiomeric to ***O1O1***/**O2O2**, but they are not interconvertible to each other because the inversion requires four transformation pathways via two structures which have a transition-metal fragment in an apical position. Therefore, the two signals observed in the ^{31}P-NMR are attributed to **O1O1**/***O2O2***/***O1O1***/**O2O2** and **O1O2**/***O1O2***.

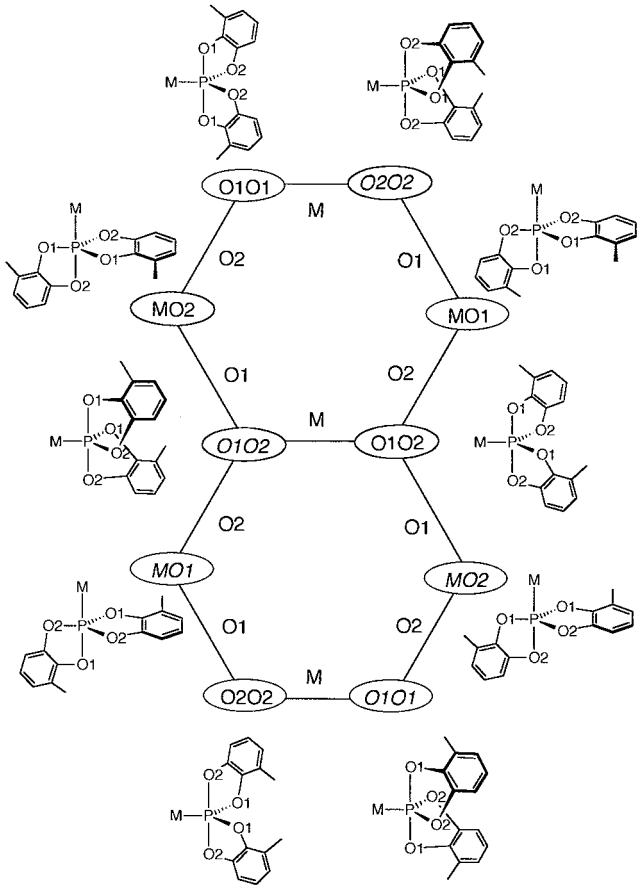

Scheme 1.

The conversion feature mentioned above is further supported by the ^{13}C-NMR data. Each isolated complex (**1b**, **2a**, and **2b**) shows three doublets due to CO. The rapid **O1O2**/***O1O2*** conversion results in the loss of the diastereotopic relationship between the two carbonyl ligands. Thus, **O1O2**/***O1O2*** would give one doublet assigned to CO. In contrast, during the **O1O1**/***O2O2*** conversion and equally the ***O1O1***/**O2O2** conversion, the phosphorus chirality is not lost, giving rise to two doublets in the ^{13}C-NMR spectra.

Lattman et al. reported the reaction of $[(PPh_3)(CO)_3Co]^-$ with $ClP(OC_6H_4O)_2$ to give cobalt phosphorane $(PPh_3)(CO)_3Co\{P(OC_6H_4O)_2\}$ [6]. We applied their method for the preparation of cobalt phosphoranes bearing two 3-methylcatecholates. The reaction of $[Co(CO)_4]^-$ with $ClP(OC_7H_6O)_2$ was first attempted to obtain $(CO)_4Co\{P(OC_7H_6O)_2\}$. However, the desired complex could not be obtained. According to the ^{31}P-NMR spectra of the reaction mixture, the added phosphorane disappeared but no symptom of cobalt phosphorane formation was observed and it was found that the reaction was not clean. In contrast, the

Table 1
Summary of crystal data for **1b**

Formula	$C_{26}R_{27}O_6PRu$
Formula weight	567.54
Crystal system	Monoclinic
Space group	$P2_1/c$
Cell constants	
a (Å)	8.9630(2)
b (Å)	13.2350(5)
c (Å)	21.9530(8)
β (°)	101.482(2)
V (Å^3)	2552.1(1)
Z	4
D_{calcd} (g cm^{-3})	1.477
μ, (cm^{-1})	7.15
Crystal size (mm)	$0.40 \times 0.25 \times 0.25$
Radiation	Mo–K$_\alpha$ ($\lambda = 0.71073$ Å)
$2\theta_{max}$ (°)	55.8
Unique data	5640
Unique data with $F_o > 3\sigma(F_o)$	4877
R	0.052
R_w	0.107

reaction of $[Co(CO)_3L]^-$ ($L = PPh_3$, PPh_2Me) with $ClP(OC_7H_6O)_2$ led to the formation of the cobalt phosphoranes (Eq. (2)). The yellow oily complexes encountered considerable difficulty in the purification process. An impurity showing a resonance at about -25 ppm in the ^{31}P-NMR spectrum could not be removed, which interfered with obtaining analytically pure spectroscopic data of **3a** and **3b**, as well as the correct elemental analysis data. However, the ^{31}P-NMR spectra are very informative. Complex **3a** shows three doublets at 48.85, 48.91, and 56.84 ppm with $J_{PP} =$ ca. 250 Hz, and **3b** shows similarly three doublets at 43.27, 51.45, and 51.56 ppm with $J_{PP} =$ ca. 250 Hz. As mentioned in the case of the iron and ruthenium phosphoranes, the cobalt complexes are expected to show two resonances assignable to the phosphorane with very close chemical shifts, which may be two doublets at 48.85 and 48.91 ppm for **3a** and those at 51.45 and 51.56 ppm for **3b**. A signal at 56.84 ppm for **3a** is assigned to PPh_3 and that at 43.27 ppm for **3b** to PPh_2Me. The upfield shift due to the change from PPh_3 to PPh_2Me is quite reasonable.

Lattman et al. reported for $(PPh_3)(CO)_3Co\{P(OC_6H_4O)_2\}$ that the ^{31}P-NMR spectrum showed an AB pattern with chemical shifts at 47 and 56 ppm with $J_{PP} = 258$ Hz. But the phosphorus assignment has not been made. Now, we can reasonably assign the signal at 47 ppm to the phosphorane. The X-ray crystal structure of the Lattman's complex revealed that the cobalt adopts a trigonal-bipyramidal geometry with three carbonyls in equatorial positions and with two phosphorus ligands in axial positions. Since the J_{PP} values are almost the same between Lattman's and our complexes, **3a** and **3b** may take a *trans* trigonal-bipyramidal structure.

2.3. Crystal structure of *1b*

The structure of **1b** was determined by X-ray diffraction (XRD) analysis. The crystal data are listed in Table 1. The orientation of one catecholate (C13–C19, O3, and O4) could be fixed, but that of the other was not. The unit cell consists of two geometrical isomers (**O2O2** and **O1O2**) and their enantiomers (***O2O2*** and ***O1O2***), and the two geometrical isomers are disordered. Therefore, the methyl position in the disordered catecholate was fixed in the two positions estimated from difference Fourier maps with a respective weight of 0.5. Eventually, **O1O1** and ***O1O1*** did not exist in the crystal, and this is presumably due to the intermolecular packing requirement. The ORTEP drawing is displayed in Fig. 1 and the selected bond distances and angles are listed in Table 2, respectively, for one of the isomers.

The X-ray structure clearly shows that **1b** is a ruthenium phosphorane complex. The ruthenium has a normal piano-stool configuration. The five-coordinate phosphorus adopts a tbp geometry with the ruthenium atom in one equatorial position. The tbp geometry is slightly distorted: the two apical bonds bend away from the ruthenium fragment (the O_{ap}–P–O_{ap} angle is 167°), and in the equatorial plane, the angles of Ru–P–O_{eq} are slightly larger (122.8 and 127.1°) than an ideal angle of 120°, though the sum of the equatorial angles is 359.2°. We previously reported the X-ray structure of ruthenium phosphorane complex, $Cp(CO)_2Ru\{P(OC_{10}H_6O)_2\}$ (**4**) [4], closely related to **1b**. The distortion from the tbp geometry around the phosphorane phosphorus was also observed for **4**: the two apical bonds bend away from the ruthenium fragment like for **1b**, but the angles of Ru–P–O_{eq} are smaller than 120°, unlike for **1b**. The larger Ru–P–O_{eq} angles for **1b** may be due to the bulky Cp* ligand. The Ru–P bond distance is slightly longer for **1b** (2.343 Å) than for **4** (2.311 Å), which may be also due to the bulky Cp* ligand. A phosphorane fragment tends to take an orientation where the σ* orbital of the 3-center-4-electron bond can accept electron density from the HOMO of the $Cp'(CO)_2M$ fragment which is shown in Fig. 2(a). Therefore, the ideal phosphorane orientation from the electronic point of view should have the same torsion angles (C1–Ru1–P1–O4 and C2–Ru1–P1–O6). However, the torsion angles for **1b** are 18.2° for C1–Ru1–P1–O4 and 72.1° for C2–Ru1–P1–O6 (Fig. 2(b)). The deviation from the ideal phosphorane orientation is larger than that for **4**, presumably due to the bulky Cp* ligand.

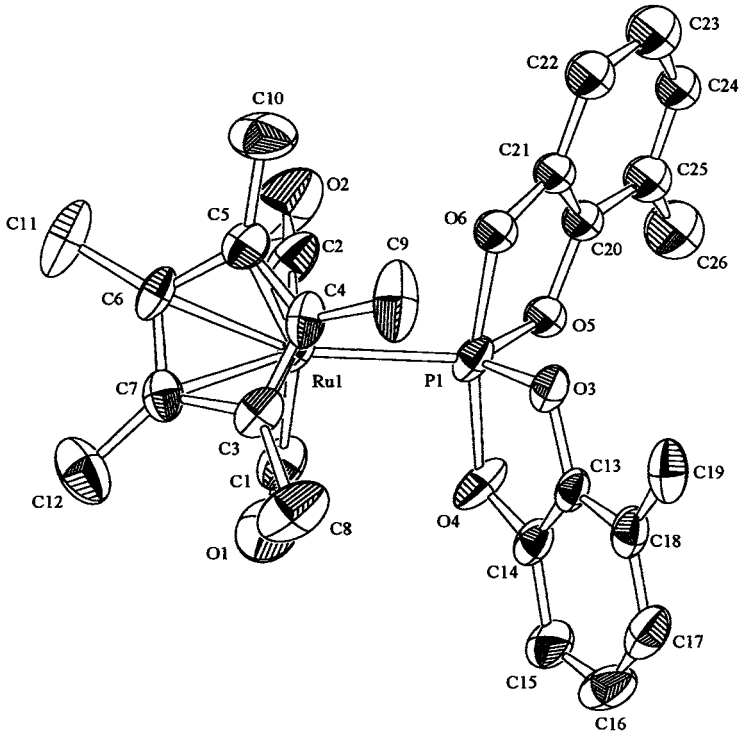

Fig. 1. ORTEP drawing of **1b** (40% probability ellipsoids), showing the numbering system. All hydrogen atoms are omitted for clarity.

2.4. Activation parameters for Berry pseudorotation process

The ^{31}P-NMR signals of metallaphosphoranes treated in this paper were temperature dependent. In the previous paper [4], the VT NMR measurements were performed for a toluene solution of **1a**. For the corresponding iron complex, **2a**, since the signals did not coalesce even at the boiling point of toluene (248 K), the solvent was changed to *p*-xylene (b.p. = 411 K). The spectral change with temperature is shown in Fig. 3. While the spectrum shows two singlets at room temperature, the signals broaden at higher temperatures and coalesce at 383 K. The broad resonance slightly sharpens as the temperature is further raised to 393 K, which was the experimental upper limit imposed by the boiling point of the solvent. The two sharp singlets were reproduced when the sample was cooled down to room temperature, indicating that no decomposition of the complex takes place during the VT NMR measurements.

This spectral behavior is explained on the basis of Berry pseudorotation around the phosphorane phosphorus. As mentioned above, **O1O1**/***O2O2*** and ***O1O1***/**O2O2** show the identical ^{31}P-NMR chemical shift, and **O1O2**/***O1O2*** shows another singlet at room temperature. Even at 286 K, the ^{31}P-NMR spectrum shows two singlets, indicating that energy barriers of pseudorotation between **O1O1** and ***O2O2*** (equally between ***O1O1*** and **O2O2**); and **O1O2** and ***O1O2*** are low. In contrast,

Table 2
Selected bond distances (Å) and angles (°) for **1b**

Bond distances			
Ru1–P1	2.343(1)	C13–C18	1.392(7)
Ru1–C1	1.887(6)	C14–C15	1.396(7)
Ru1–C2	1.896(5)	C15–C16	1.367(9)
P1–O3	1.647(4)	C16–C17	1.39(1)
P1–O4	1.784(4)	C17–C18	1.383(8)
P1–O5	1.701(8)	C18–C19	1.480(9)
P1–O6	1.867(8)	C20–C21	1.37(1)
O1–C1	1.138(7)	C20–C25	1.37(2)
O2–C2	1.137(7)	C21–C22	1.41(2)
O3–C13	1.392(5)	C22–C23	1.34(2)
O4–C14	1.334(6)	C23–C24	1.49(2)
O5–C20	1.38(1)	C24–C25	1.36(2)
O6–C21	1.35(1)	C25–C26	1.45(2)
C13–C14	1.363(7)		
Bond angles			
P1–Ru1–C1	90.4(2)	O5–P1–O6	83.8(4)
P1–Ru1–C2	88.6(2)	P1–O3–C13	113.8(3)
C1–Ru1–C2	93.8(3)	P1–O4–C14	112.7(4)
Ru1–P1–O3	122.8(1)	P1–O5–C20	118.1(7)
Ru1–P1–O4	96.9(2)	P1–O6–C21	114.7(7)
Ru1–P1–O5	127.1(2)	Ru1–C1–O1	175.0(5)
Ru1–P1–O6	94.6(3)	Ru1–C2–O2	175.4(5)
O3–P1–O4	88.6(2)	O3–C13–C14	113.1(4)
O3–P1–O5	109.3(3)	O4–C14–C13	111.5(4)
O3–P1–O6	81.5(3)	O5–C20–C21	112.3(9)
O4–P1–O5	92.8(3)	O6–C21–C20	111.3(9)
O4–P1–O6	167.7(3)		

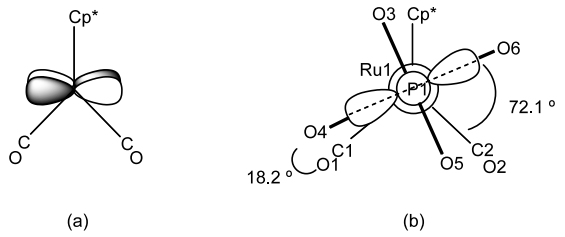

Fig. 2. (a) HOMO of the $Cp^*(CO)_2M$. (b) Newman projection along the P1–Ru1 bond for **1b**.

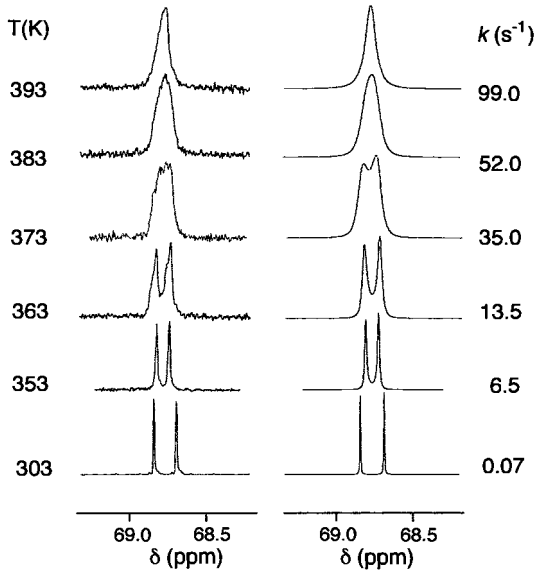

Fig. 3. Variable-temperature experimental (left) and simulated (right) ^{31}P-NMR spectra of **2a**.

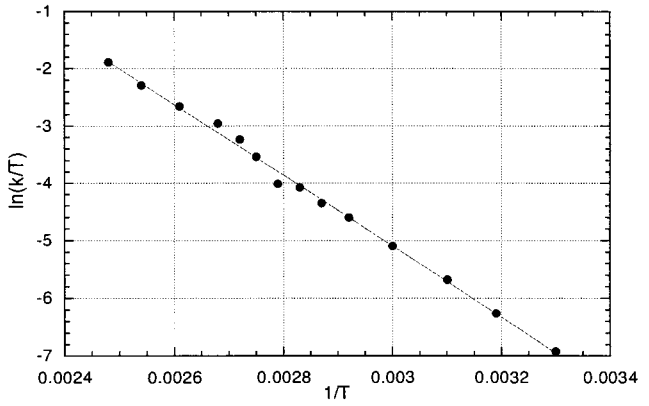

Fig. 4. Eyring plot for the rotation of the phosphorane ligand along the Fe–P axis in **2a** derived from variable-temperature NMR data.

the two singlets coalesce into one broad resonance at 383 K. This means that isomerization between **O1O1**/***O2O2*** and **O1O2**/***O1O2*** (equally between ***O1O1***/**O2O2** and **O1O2**/***O1O2***) takes place faster than the NMR time scale at temperatures higher than 383 K. Line shape analysis yielded calculated spectra in good agreement with the experimental VT NMR data and afforded activation parameters via an Eyring analysis (Fig. 4) [7].

Similar spectral changes were observed for **2b**, **3a**, and **3b**. For the Cp* derivatives, **1b** and **2b**, since higher temperature was required to observe the coalescence temperature, *n*-butyl benzene (b.p. = 456 K) was used as a solvent. Even in the solvent, the signals for **1b** did not coalesce. For **3a** and **3b**, in contrast, a temperature lower than a room temperature was requested, and then THF was used as a solvent. Although **3a** and **3b** have not been isolated in a pure form, several VT NMR measurements were performed for samples containing the impurity in a different ratio (10–30% based on the cobalt phosphorane) and the same results were obtained. Therefore, it can be said that the impurity does not affect the energy barriers to Berry pseudorotation.

Activation parameters thus obtained are summarized in Table 3. Although the $\Delta H^{\neq}$ for **1b** could not be obtained due to a higher coalescence temperature than the boiling point of the solvent used, the $\Delta H^{\neq}$ could be estimated to be greater than 67.9 kJ mol^{-1} estimated for **2b** under the same conditions.

The activation parameters evaluated here correspond to the isomerization between **O1O1**/***O2O2*** and **O1O2**/***O1O2***, and equally to that between ***O1O1***/**O2O2** and **O1O2**/***O1O2*** (see Scheme 1). In any case, the isomerization takes place via a relatively unstable isomer having a transition metal fragment in an apical position. The isomer is depicted in Fig. 5 where (a) shows the equatorial plane and (b) is a plane containing a transition

Table 3
Activation parameters $\Delta H^{\neq}$, $\Delta S^{\neq}$ and $\Delta G^{\neq}$ for **1a**,* **1b**, **2a**, **2b**, **3a**, and **3b**

Complex	$\Delta H^{\neq}$ (kJ mol^{-1})	$\Delta S^{\neq}$ (J mol^{-1} K^{-1})	$\Delta G^{\neq}$ (kJ mol^{-1})
1a	42.1 ± 0.5	-91.1 ± 1.6	73.1 ± 0.7 (340 K)
1b	>67.9	–	–
2a	51.4 ± 0.8	-85.7 ± 2.5	84.2 ± 1.3 (383 K)
2b	67.9 ± 1.4	-51.8 ± 3.7	89.7 ± 2.1 (420 K)
3a	38.6 ± 0.3	-96.5 ± 1.1	67.8 ± 0.5 (303 K)
3b	38.5 ± 0.2	-97.1 ± 0.8	67.9 ± 0.3 (303 K)

* See Ref. [4].

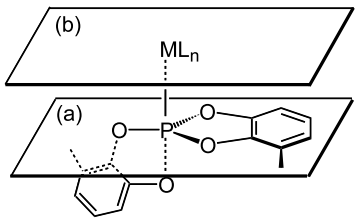

Fig. 5. One of the isomers in a process of pseudorotation of metallaphosphorane. (a) An equatorial plane; (b) a plane containing a transition metal in the apical position and parallel to (a).

metal in the apical position and parallel to (a). With interconversion via the unstable isomer, two factors should be considered: (i) a steric factor (steric repulsion between equatorial substituents on (a) and an apical transition metal fragment on (b)) and (ii) an electronic factor (π-back donation from a transition metal to a phosphorane fragment which has been pointed out to be important for $Cp(CO)_2M$(phosphorane) (M = Fe and Ru)) [4,5,8].

The point which should be noted first in Table 3 is that the activation parameters for **3a** and **3b** are the same. The factor (i) seems to be the same for **3a** and **3b** because the phosphine on the cobalt may keep the position trans to the phosphorane during the pseudorotation. Therefore, the same activation parameters derived from **3a** and **3b** show that the extent of π-back donation from $Co(CO)_3L$ to the phosphorane is the same in **3a** and **3b**, indicating that the π-back donation is weak if any.

The next point noted is that $\Delta H^{\pm}$ is greater for the iron and ruthenium complexes than for the cobalt complexes. This can be explained from both factors (i) and (ii). Let us consider the factor (ii) first. The π-back donation from a filled d orbital to empty σ* orbitals of phosphorane apical bonds have been reported to stabilize metallaphosphoranes having a transition metal fragment in an equatorial position, such as $Cp(CO)_2M$(phosphorane) (M = Fe, Ru). However, the π-back donation is not expected for the isomer shown in Fig. 5. Therefore, the pseudorotation, for example from **O1O1** to **MO2**, requests more energy for the Fe and Ru complexes. Next, let us consider the factor (i). The Cp ligand protrudes below (b) in Fig. 5, which leads to considerable steric repulsion between the Cp ligand and the equatorial substituents giving a greater activation energy. The effect is more prominent for bulkier Cp* derivatives, consistent with the greater $\Delta H^{\neq}$ (**1a** vs. **1b** and **2a** vs. **2b**; greater than 16.5 kJ mol^{-1} compared with the corresponding Cp derivative).

Finally let us compare $\Delta H^{\neq}$s for the Ru and Fe complexes. It has been reported that the $Cp(CO)_2Ru$ fragment has stronger π-back donation ability than the corresponding iron fragment [4]. Therefore, $\Delta H^{\neq}$ is expected to be greater for a ruthenium complex than for an iron complex. Actually $\Delta H^{\neq}$ for **1b** is greater than that for **2b**. However, $\Delta H^{\neq}$s for **1a** and **2a** show the opposite tendency. For $Cp'(CO)_2M$(phosphorane) (M = Ru, Fe), the Ru–P bond distances (2.311–2.377 Å) are longer than the Fe–P bond distances (2.272–2.291 Å) [4,5b]. Therefore, steric repulsion is expected to be smaller for **1a** than for **2a**, leading to smaller $\Delta H^{\neq}$ for **1a** than for **2a**. $\Delta H^{\neq}$s for **1a** and **1b** (the difference is only 9.3 kJ mol^{-1}) may be the results of a critical balance of the two antagonistic (steric and electronic) factors.

3. Experimental

3.1. General remarks

All reactions were carried out under an atmosphere of dry nitrogen by using standard Schlenk tube techniques. All solvents were purified by distillation: ether, THF, benzene, toluene, *p*-xylene, and *n*-butylbenzene were distilled from sodium–benzophenone, hexane and pentane were distilled from sodium metal, and CH_2Cl_2 was distilled from P_2O_5. They were stored under an N_2 atmosphere. Other reagents were used without further purification. $Cp(CO)_2Fe\{P(OPh)_3\}]PF_6$ [9], $Cp^*(CO)_2Fe\{P(OPh)_3\}]PF_6$ [9], $Cp^*(CO)_2RuCl$ [10], $[Co(CO)_3(PPh_3)]_2$ [11], $[Co(CO)_3(PMePh_2)]_2$ [11], and $ClP(OC_7H_6O)_2$ [12,13] were prepared according to the respective published procedures with some modifications.

IR spectra were recorded on a Shimadzu FTIR-8100A spectrometer. A JEOL LA-300 multinuclear spectrometer was used to obtain ^{1}H-, ^{13}C-, and ^{31}P-NMR spectra. ^{1}H- and ^{13}C-NMR data were referenced to $Si(CH_3)_4$ as an internal standard. ^{31}P-NMR data were referenced to 85% H_3PO_4 as an external standard. Elemental analyses were performed on a Perkin–Elmer 2400CHN elemental analyzer.

3.2. Preparation of $[Cp^*(CO)_2Ru\{P(OPh)_3\}]BF_4$

A solution of $Cp^*(CO)_2RuCl$ (613 mg, 1.87 mmol) and $P(OPh)_3$ (560 mg, 1.87 mmol) in CH_2Cl_2 (50 ml) was added to a suspension of $AgBF_4$ (364 mg, 1.87 mmol) in CH_2Cl_2 (20 ml). The mixture was stirred for 10 h at room temperature (r.t.). After filtration to remove AgCl formed, the solvent was removed from the filtrate under reduced pressure to give a yellow powder, which was washed with benzene and then ether. Crystallization from CH_2Cl_2–hexane gave colorless crystals (967 mg, 1.40 mmol, 75%). Anal. Calc. for $C_{30}H_{30}BF_4O_5PRu$: C, 52.27; H, 4.39. Found: C, 52.02; H, 4.15%. IR (ν_{CO}, cm^{-1}, in CH_2Cl_2): 2066, 2022. ^{1}H-NMR (δ, in $CDCl_3$): 1.97 (d, $J_{PH} = 3.1$ Hz, 15H, $C_5(CH_3)_5$), 7.13 (d, $J_{HH} = 7.8$ Hz, 6H, *o*-C_6H_5), 7.25 (m, 3H, *p*-C_6H_5), 7.40 (t, $J_{HH} = 7.7$ Hz, 6H, *m*-C_6H_5). ^{13}C-NMR (δ, in $CDCl_3$): 9.62 (s, $C_5(CH_3)_5$), 104.34 (d, $J_{PC} = 1.9$ Hz, $C_5(CH_3)_5$), 120.22 (d, $J_{PC} = 5.0$ Hz, *o*-C_6H_5), 126.39 (s, *p*-C_6H_5), 130.40 (s, *m*-C_6H_5), 149.80 (d, $J_{PC} = 9.9$ Hz, *ε*-C_6H_5), 195.11 (d, $J_{PC} = 21.8$ Hz, CO). ^{31}P-NMR (δ, in $CDCl_3$): 132.36 (s).

3.3. Preparation of $Cp^*(CO)_2Ru\{P(OC_7H_6O)_2\}$ (**1b**)

A solution of $[Cp^*(CO)_2Ru\{P(OPh)_3\}]BF_4$ (371 mg, 0.54 mmol) in THF (5 ml) was added to a solution of 3-methylcatechol (134 mg, 1.08 mmol) and Et_3N (0.075 ml, 0.54 mmol) in THF (5 ml). The mixture was stirred

for 3 h at 55 °C, and the volatile compounds were removed under reduced pressure. The yellow residue was extracted with ether (20 ml × 2), and the ether extract was evaporated to dryness. Crystallization from ether/hexane gave pale yellow crystals of **1b** (200 mg, 0.35 mmol, 66%). Anal. Calc. for $C_{26}H_{27}O_6PRu$: C, 55.02; H, 4.80. Found: C, 54.72; H, 4.70%. IR (ν_{CO}, cm^{-1}, in THF): 2034, 1983. ^{1}H-NMR (δ, in $CDCl_3$): 1.92 (d, $J_{PH} = 3.3$ Hz, 8H, $C_5(CH_3)_5$), 1.93 (d, $J_{PH} = 3.3$ Hz, 7H, $C_5(CH_3)_5$), 2.27 (s, 6H, $OC_6H_3(CH_3)O$), 6.60–6.78 (m, 6H, $OC_6H_3(CH_3)O$). ^{13}C-NMR (δ, in $CDCl_3$): 10.25 (s, $C_5(CH_3)_5$), 15.35 (s, $OC_6H_3(CH_3)O$), 101.54 (d, $J_{PC} = 3.1$ Hz, $C_5(CH_3)_5$), 101.57 (d, $J_{PC} = 1.9$ Hz, $C_5(CH_3)_5$), 107.56 (d, $J_{PC} = 8.7$ Hz, $OC_6H_3(CH_3)O$), 107.82 (d, $J_{PC} = 9.3$ Hz, $OC_6H_3(CH_3)O$), 119.33 (s, $OC_6H_3(CH_3)O$), 119.59 (s, $OC_6H_3(CH_3)O$), 119.84 (d, $J_{PC} = 7.5$ Hz, $OC_6H_3(CH_3)O$), 120.00 (d, $J_{PC} = 8.7$ Hz, $OC_6H_3(CH_3)O$), 121.98 (s, $OC_6H_3(CH_3)O$), 122.32 (s, $OC_6H_3(CH_3)O$), 143.98 (s, $OC_6H_3(CH_3)O$), 144.30 (s, $OC_6H_3(CH_3)O$), 144.72 (s, $OC_6H_3(CH_3)O$), 145.10 (s, $OC_6H_3(CH_3)O$), 198.20 (d, $J_{PC} = 24.2$ Hz, CO), 198.39 (d, $J_{PC} = 23.6$ Hz, CO), 198.55 (d, $J_{PC} = 23.6$ Hz, CO). ^{31}P-NMR (δ, in $CDCl_3$): 50.57 (s), 51.18 (s).

3.4. Preparation of $Cp(CO)_2Fe\{P(OC_7H_6O)_2\}$ (2a)

A treatment of $[Cp(CO)_2Fe\{P(OPh)_3\}]PF_6$ (443 mg, 0.70 mmol) with 3-methylcatechol (174 mg, 1.40 mmol) and Et_3N (0.39 ml, 2.80 mmol) in a similar manner to that of **1b** gave a yellow powder of **2a** (142 mg, 0.31 mmol, 45%). Anal. Calc. for $C_{21}H_{17}O_6PFe$: C, 55.78; H, 3.79. Found: C, 55.55; H, 3.76%. IR (ν_{CO}, cm^{-1}, in $CDCl_3$): 2046, 1998. ^{1}H-NMR (δ, in $CDCl_3$): 2.27 (s, 3H, $OC_6H_3(CH_3)O$), 2.28 (s, 3H, $OC_6H_3(CH_3)O$), 5.02 (d, 5H, $J_{PH} = 0.8$ Hz, C_5H_5), 6.64–6.82 (m, 6H, $OC_6H_3(CH_3)O$). ^{13}C-NMR (δ, in $CDCl_3$): 15.25 (s, $OC_6H_3(CH_3)O$), 85.17 (s, C_5H_5), 107.62 (d, $J_{PC} = 8.7$ Hz, $OC_6H_3(CH_3)O$), 107.87 (d, $J_{PC} = 9.4$ Hz, $OC_6H_3(CH_3)O$), 119.80 (s, $OC_6H_3(CH_3)O$), 120.03 (s, $OC_6H_3(CH_3)O$), 120.14 (d, $J_{PC} = 10.6$ Hz, $OC_6H_3(CH_3)O$), 120.28 (d, $J_{PC} = 11.2$ Hz, $OC_6H_3(CH_3)O$), 122.38 (s, $OC_6H_3(CH_3)O$), 122.72 (s, $OC_6H_3(CH_3)O$), 143.84 (s, $OC_6H_3(CH_3)O$), 144.12 (s, $OC_6H_3(CH_3)O$), 144.51 (s, $OC_6H_3(CH_3)O$), 144.93 (s, $OC_6H_3(CH_3)O$), 210.20 (d, $J_{PC} = 44.1$ Hz, CO), 210.26 (d, $J_{PC} = 44.7$ Hz, CO), 210.27 (d, $J_{PC} = 44.1$ Hz, CO). ^{31}P-NMR (δ, in $CDCl_3$): 70.97 (s), 71.59 (s).

3.5. Preparation of $Cp^*(CO)_2Fe\{P(OC_7H_6O)_2\}$ (2b)

A treatment of $[Cp^*(CO)_2Fe\{P(OPh)_3\}]PF_6$ (559 mg, 0.80 mmol) with 3-methylcatechol (198 mg, 1.59 mmol) and Et_3N (0.11 ml, 0.96 mmol) in a similar manner to that of **1b** gave yellow crystals of **2b** (263 mg, 0.50 mmol, 63%). Anal. Calc. for $C_{26}H_{27}O_6PFe$: C, 59.79; H, 5.21. Found: C, 59.77; H, 5.24%. IR (ν_{CO}, cm^{-1}, in THF): 2024, 1975. ^{1}H-NMR (δ, in $CDCl_3$): 1.80 (d, $J_{PH} = 1.7$ Hz, 15H, $C_5(CH_3)_5$), 2.25 (s, 6H, $OC_6H_3(CH_3)O$), 6.57–6.76 (m, 6H, $OC_6H_3(CH_3)O$). ^{13}C-NMR (δ, in $CDCl_3$): 9.84 (s, $C_5(CH_3)_5$), 15.28 (s, $OC_6H_3(CH_3)O$), 97.92 (s, $C_5(CH_3)_5$), 107.32 (d, $J_{PC} = 6.8$ Hz, $OC_6H_3(CH_3)O$), 107.70 (d, $J_{PC} = 8.1$ Hz, $OC_6H_3(CH_3)O$), 118.80 (s, $OC_6H_3(CH_3)O$), 119.33 (s, $OC_6H_3(CH_3)O$), 119.35 (d, $J_{PC} = 6.8$ Hz, $OC_6H_3(CH_3)O$), 119.63 (d, $J_{PC} = 6.8$ Hz, $OC_6H_3(CH_3)O$), 121.69 (s, $OC_6H_3(CH_3)O$), 122.27 (s, $OC_6H_3(CH_3)O$), 144.81 (d, $J_{PC} = 2.5$ Hz, $OC_6H_3(CH_3)O$), 145.01 (s, $OC_6H_3(CH_3)O$), 145.65 (d, $J_{PC} = 2.5$ Hz, $OC_6H_3(CH_3)O$), 145.95 (d, $J_{PC} = 1.9$ Hz, $OC_6H_3(CH_3)O$), 212.08 (d, $J_{PC} = 41.6$ Hz, CO), 212.33 (d, $J_{PC} = 41.0$ Hz, CO), 212.63 (d, $J_{PC} = 41.0$ Hz, CO). ^{31}P-NMR (δ, in $CDCl_3$): 74.63 (s), 75.16 (s).

3.6. Preparation of $(PPh_3)(CO)_3Co\{P(OC_7H_6O)_2\}$ (3a)

$[Co(PPh_3)(CO)_3]_2$ (257 mg, 0.32 mmol) was dissolved in THF (15 ml) and then $NaK_{2.8}$ (168 mg, 1.27 mmol) was added. After 45 min stirring at r.t., the mixture was filtered to remove unreacted $NaK_{2.8}$ and the insoluble materials. The solution containing $K[Co(PPh_3)(CO)_3]$ was cooled at −78 °C and $ClP(OC_7H_6O)_2$ (190 mg, 0.61 mmol) was added. The reaction mixture was warmed to r.t., then the volatile solvent was removed to give a brown oil. After washing the oil with hexane (50 ml × 3), ether (10 ml) was added to extract **3a**. The solvent was removed from the ether extract under reduced pressure to give a yellow oil (**3a**) with some impurity. ^{31}P-NMR (δ, in $CDCl_3$): 48.85 (d, $J_{PP} = 249.9$ Hz, phosphorane), 48.91 (d, $J_{PP} = 238.1$ Hz, phosphorane), 56.84 (d, $J_{PP} = 252.5$ Hz, PPh_3).

3.7. Preparation of $(PMePh_2)(CO)_3Co\{P(OC_7H_6O)_2\}$ (3b)

The complex was prepared from $[Co(PPh_2Me)(CO)_3]_2$ in a manner similar to that of **3a**. The yellow oil of **3b** has some impurity, which could not be removed completely. ^{31}P-NMR (δ, in $CDCl_3$): 43.27 (d, $J_{PP} = 246.7$ Hz, PPh_2Me), 51.45 (d, $J_{PP} = 247.4$ Hz, phosphorane), 51.56 (d, $J_{PP} = 246.7$ Hz, phosphorane).

3.8. X-ray structure determination for 1b

Crystallographic and experimental details of X-ray crystal structure analysis for **1b** are given in Table 1. A suitable crystal of **1b** was mounted on a glass fiber. All measurements were made on a MacScience DIP2030 imaging plate area detector with graphite monochromated Mo–K_α radiation ($\lambda = 0.71073$ Å). The crystal-to-detector distance was 100 mm with the detector at the zero swing position. Readout was performed in the

0.050 mm pixel mode. The data were collected at a temperature of 200 ± 1 K to a maximum 2θ value of 55.8°. A total of 90 oscillation images were collected, each being exposed for 4.0 min with an oscillation angle of 2.0°. Cell parameters and intensities for the reflection were estimated by the program packages of MACDENZO [14].

The structure was solved by direct methods [15] and expanded using Fourier techniques [16]. Non-hydrogen atoms except for the disordered $OC_6H_3(CH_3)O$ were refined anisotropically, while the rest were refined isotropically. Hydrogen atoms were included but were not refined. The final cycle of full-matrix least-squares refinement was calculated on the basis of 4877 observed reflections ($F_o > 3\sigma(F_o)$) and 299 variable parameters, and converged (the largest parameter shift was less than 0.19 times its estimated S.D.) with unweighted and weighted agreement factors $R = 0.052$ and $R_w = 0.104$. Neutral atom scattering factors were taken from Cromer and Waber [17]. All calculations were performed on an SGI Indy O_2 computer using the program system TEXSAN crystallographic software package of Molecular Structure Corporation [18].

Acknowledgements

This work was supported by a Grant-in-Aid for Science Research (Number 12640539 and 12640540) from the Ministry of Education, Science, Sports and Culture of Japan.

References

[1] K.Y. Akiba (Chapter 2), T. Kawashima (Chapter 6), Y. Yamamoto, K.Y. Akiba (Chapter 9), in: K.Y. Akiba (Ed.), Chemistry of Hypervalent Compounds, Wiley VCH, New York, 1999.
[2] (a) J. Emsley, D. Hall, The Chemistry of Phosphorus, Harper & Row, New York, 1976;
(b) R.R. Holmes, Pentacoordinated Phosphorus, ACS Monograph Series 175 and 176, vols. I and II, American Chemical Society, Washington, DC, 1980.
[3] (a) J. Moc, K. Morokuma, J. Am. Chem. Soc. 117 (1995) 11790, and references cited therein;
(b) T. Uchimura, M. Uebayasi, T. Hirose, S. Tsuzuki, A. Yliniemelä, K. Tanabe, K. Taira, J. Org. Chem. 61 (1996) 1608;
(c) S. Kojima, K. Kajiyama, M. Nakamoto, K.Y. Akiba, J. Am. Chem. Soc. 118 (1996) 12866.
[4] H. Nakazawa, K. Kawamura, K. Kubo, K. Miyoshi, Organometallics 18 (1999) 2961.
[5] (a) H. Nakazawa, K. Kubo, K. Miyoshi, J. Am. Chem. Soc. 115 (1993) 5863;
(b) K. Kubo, H. Nakazawa, T. Mizuta, K. Miyoshi, Organometallics 17 (1998) 3522.
[6] M. Lattman, S.A. Morse, A.H. Cowley, J.G. Lasch, N.C. Norman, Inorg. Chem. 14 (1985) 1364.
[7] (a) DMNR5: D.S. Stephenson, G. Binch, Program 365, Quantum Chemistry Program Exchange, Indiana University, Bloomington, IN 47405;
(b) DNMR5 (IBM-PC version): C.B. Lemaster, L.C. leMaster, N.S. true, Program QCMP 059, Quantum Chemistry Program Exchange, Indiana University, Bloomington, IN 47405.
[8] S.K. Chopra, J.C. Martin, Heteroat. Chem. 2 (1991) 71.
[9] D. Catheline, D. Astruc, Organometallics 3 (1984) 1094.
[10] T. Blockmore, J.D. Cotton, M.I. Bruce, F.G.A. Stone, J. Chem. Soc. A (1968) 2931.
[11] A.R. Manning, J. Chem. Soc. A (1968) 1135.
[12] F. Ramirez, A.J. Bigler, C.P. Smith, Tetrahedron 24 (1968) 5041.
[13] K.B. Dillon, R.N. Reev, T.C. Waddington, J. Chem. Soc., Dalton Trans. (1978) 1465.
[14] MACDENZO: D. Gewirth, (with the cooperation of the program authors Z. Otwinowski, W. Minor), The MACDENZO Manual—A Description of the Program DENZO, XDISPLAYF, and SCALEPACK, Yale University, New Haven, CT, 1995.
[15] SIR92: A. Altomare, M.C. Burla, M. Camalli, M. Cascarano, C. Giacovazzo, A. Guagliardi, G. Polidori, J. Appl. Crystallogr. 27 (1994) 435.
[16] DIRDIF94: P.T. Beurskens, G. Admiraal, G. Beurskens, W.P. Bosman, R. de Gelder, R. Israel, J.M.M. Smits, The DIRDIF-94 Program System, Technical Report of the Crystallography Laboratory; University of Nijmegen, The Netherlands, 1994.
[17] D.T. Cromer, J.T. Waber, International Tables for X-ray Crystallography, vol. IV, The Kynoch Press, Birmingham, England, 1974; table 2.2 A.
[18] TEXSAN: Single-Crystal Structure Analysis Software, version 1.6, Molecular Structure Corporation, The Woodlands, TX, 1993.